

# A Bending Filament Model for Fluid Rope Coiling

Shin-ichiro Nagahiro

*Department of Mechanical Engineering, Miyagi National College of Technology, Miyagi 981-1239, Japan*

Yoshinori Hayakawa

*Department of Physics, Tohoku University, Aoba-ku, Sendai, 980-8578, Japan*

(Dated: June 21, 2024)

A simple model is proposed for the buckling and coiling instability of a viscous “fluid rope” falling on a plane. By regarding a fluid rope as a one-dimensional flow, this model accounts for only the axial and shared viscous forces. It was found that our model successfully reproduces several experiments with no adjustable parameters, such as the existence of three distinct coiling regimes reported in *Phys. Rev. Lett.* **93**, 214502 (2004). Our model allows for the discussion of unsteady motion. In addition, the critical Reynolds number for the coil-uncoil transition and  $\text{Re}^* \simeq 3$  for the no gravity condition were obtained. An expression for the critical fall height at which the coiling frequency changes from a decrease to increase was phenomenologically derived.

PACS numbers:

In the low Reynolds number regime, the dynamics of viscous fluid confined in rigid boundaries do not exhibit complex behavior because the possible eigenmodes are limited. However, if the fluid interface can move freely and deform largely, this is not the case, and rich variety of dynamics can emerge *below* a critical Reynolds number. Backing and coiling instabilities of fluid jets are examples of such systems, and have been studied for several decades in the laboratory [1, 2, 3, 4, 5, 6]. A fluid rope and coiling can also be observed in daily life, such as when honey is poured from a teaspoon onto toast.

Although the mathematical treatment of a largely deformed fluid is not theoretically straightforward, the conditions for the onset of coiling instability have been thoroughly examined in terms of linear stability analysis with some simplifications and assumptions [7, 8, 9].

Recently, Ribe derived the differential equations to describe steady state coiling for a very thin rotating rope, and showed the numerical solutions for various conditions [10]. His analysis reveals that the steady solution is multi-valued so that there might be a discontinuity in the selected coiling frequency.

Ribe also demonstrated the existence of three distinct coiling modes; viscous, gravitational, and inertial regimes. Phenomenologically, one could understand that buckling and coiling instability occurs under the mechanical balance between the driving force of a steady flow and the internal stress due to viscosity. Signifying the magnitudes of force for fluid injection as  $F_P$ , the gravitational force acting to fluid as  $F_G$ , the inertial force as  $F_I$ , and the yielding stress due to viscosity as  $F_V$ , the viscous coiling regime corresponds the condition  $F_P \sim F_V$ , the gravitational coiling regime  $F_G \sim F_V$ , and the inertial coiling regime  $F_I \sim F_V$ , respectively. Dimensional analysis allows for the estimation of the coiling frequencies

for each regime as

$$\Omega_V = \frac{Q}{Ha^2}, \quad (1)$$

$$\Omega_G = \left( \frac{gQ^3}{\nu a^8} \right)^{1/4}, \quad (2)$$

$$\Omega_I = \left( \frac{Q^4}{\nu a^{10}} \right)^{1/3}, \quad (3)$$

where  $Q$  is the flow rate,  $H$  is the fall height,  $\nu$  is the kinetic viscosity,  $g$  is the gravitational acceleration, and  $a$  is the radius of the rope.

Although these studies seem to succeed in giving the onset of coiling with infinitesimal amplitude and steady coiling frequencies, in order to discuss the stability and further turbulent states, a numerical model is still needed that can describe the entire dynamics including transient states with fewer computational costs.

In this paper, an alternative numerical model for a small deflection in a fluid rope is proposed and coiling frequency as a function of fall height is investigated. In addition, the critical Reynolds number below which fluid rope will buckle and coil is discussed, as well as the transition height from viscous to gravitational coiling.

Figure 1 is a schematic view of a fluid rope injected from an orifice at a sufficient height. We fix the origin of the reference frame at the point where the rope begins to coil and align the  $z$  axis parallel to gravity  $\mathbf{g}$ . In the present model, we require a “steady coiling state” in which the upward growth speed of the coil is balanced by the speed of downward flow at the top of coil ( $= w_b$ ), i.e. the point at which the rope changes to the coil does not move.

We consider a uniform flow within the rope and write the flow velocity as  $\mathbf{w} = w\mathbf{n}$ , where  $\mathbf{n} = (n_x, n_y, n_z)$  is the unit vector tangential to the rope. Since we restrict the present model to the case of slight deflection, the vector  $\mathbf{n}$  is almost parallel to the  $z$  axis. We only takes account of the first order of  $n_x$  and  $n_y$ , and replace the

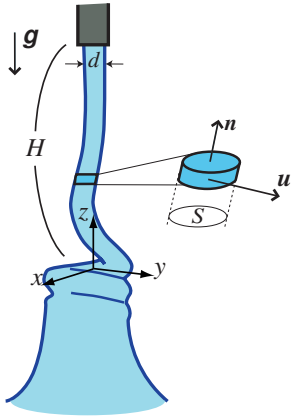


FIG. 1: A schematic view of a fluid rope coiling.

derivative with respect to  $\mathbf{n}$  by the derivative with respect to  $z$ . In this manner, the axial stress is written as  $\sigma_n = 3\eta\partial w/\partial z$ , where  $3\eta$  is the extension (or compression) viscosity [11]. The flow velocity obeys

$$\left(\frac{\partial}{\partial t} + w\frac{\partial}{\partial z}\right)w = \frac{1}{\rho S}\frac{\partial}{\partial z}(S\sigma_n) - g, \quad (4)$$

where  $\partial/\partial t$  is the time derivative,  $\rho$  is the density and  $S$  is the rope's cross-sectional area taken to be parallel to  $xy$  plane. We determine  $S$  by solving the following continuity equation

$$\frac{\partial S}{\partial t} = \frac{\partial}{\partial z}(Sw). \quad (5)$$

In order to describe the deformation of the fluid rope, we divide the rope into thin cylindrical elements that move  $x$  and  $y$  direction, as shown in Fig. 1. Denoting the position of the element  $\mathbf{q} = (q_x, q_y)$  and velocity  $\mathbf{u} = (u_x, u_y)$ , these quantities obey

$$\left(\frac{\partial}{\partial t} + w\frac{\partial}{\partial z}\right)q_i = u_i, \quad (6)$$

where  $i = x$  and  $y$ . The viscous shear stress between two neighboring elements is  $\sigma_i = \eta\partial(u_i + wn_i)/\partial z$ , and the  $i$ th component of the axial stress is  $n_i\sigma_n$ . Therefore, we obtain the equation of motion for a cylindrical element as

$$\left(\frac{\partial}{\partial t} + w\frac{\partial}{\partial z}\right)u_i = \frac{1}{\rho S}\frac{\partial}{\partial z}\{S(\sigma_i + n_i\sigma_n)\}. \quad (7)$$

Next, we discuss the boundary conditions of the present model. At the injection point  $z = H$ , the fluid rope is fixed, or

$$q_i(H) = 0, \quad u_i(H) = 0, \quad (8)$$

and  $S(H) = \pi d^2/4$ , with  $d$  as the diameter of the orifice. We neglect the relaxation of Poiseuille flow to plug flow

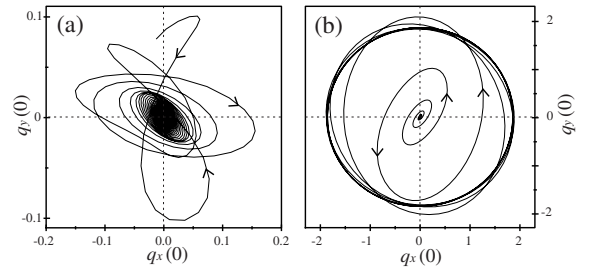


FIG. 2: Trajectories of the bottom of the model rope starts at  $t = 0$ : (a) Trajectory in the case that straight flow is stable at the steady state ( $\text{Re} = 10.0$ ,  $\text{Fr} = 1.0$ ,  $H/d = 10$ ). (b) Trajectory of circular coiling ( $\text{Re} = 1.0$ ,  $\text{Fr} = 1.0$ ,  $H/d = 10$ ).

in the neighborhood of the orifice, and assume a uniform flow at the injection point:

$$w(H) = -w_{\text{in}}. \quad (9)$$

Next, let us turn to the boundary conditions at  $z = 0$ . We assume that

$$q'_i(0) = 0, \quad u'_i(0) = 0, \quad (10)$$

where a prime indicates a derivative with respect to  $z$ . The flow velocity at  $z = 0$  should be equal to the speed of the downward flow at the top of coil. Let  $w_{\text{max}}$  be the maximum of  $|w(z)|$  at an instant. It is experimentally found that  $w_b \approx -0.13w_{\text{max}}$ , which relation is fairly independent of flow conditions such as the viscosity of the liquid, the orifice diameter or the fall height [12]. We therefore require the following time dependent boundary condition

$$w(0) = -0.13w_{\text{max}}. \quad (11)$$

We numerically solve the equations (4), (5), (6) and (7) setting a straight flow,  $w(z) = -1$ ,  $S(z) = \pi/4$ ,  $q_i(z) = 0$ , and  $u_i(z) = 0$  as an initial condition. For  $q_i(z)$ , a small roughness with amplitude of  $0.01d$  is given. The tangent vector  $\mathbf{n}$  is calculated from the derivative of  $\mathbf{q}$  with respect to  $z$  as  $\mathbf{n} = (\partial q_x/\partial z, \partial q_y/\partial z, 1)/C$  with  $C = \sqrt{(\partial q_x/\partial z)^2 + (\partial q_y/\partial z)^2 + 1}$ .

The control parameters of the numerical calculations are the Reynolds number  $\text{Re} = \rho d|w_{\text{in}}|/\eta$ , the Froude number  $\text{Fr} = w_{\text{in}}^2/gd$  and the fall height  $H/d$ . The other parameters are fixed as  $d = \rho = 1$  and  $w_{\text{in}} = -1$ .

Figure 2 shows trajectories of  $\mathbf{q}$  in the plane  $z = 0$ . Simulation movies are available[13]. In the case that  $\text{Re}$  is sufficiently large, the axial stagnation flow is stable, thus the trajectory converges to the origin, as shown in Fig. 2(a). Such an axial flow could be appear to be under no gravity condition. When we set  $\text{Re}$  smaller than a critical value, the flow starts to oscillate and a circular trajectory would appear at the steady state (Fig. 2(b)).

Most of experimental works on fluid rope coiling discuss coiling frequency as a function of the fall height

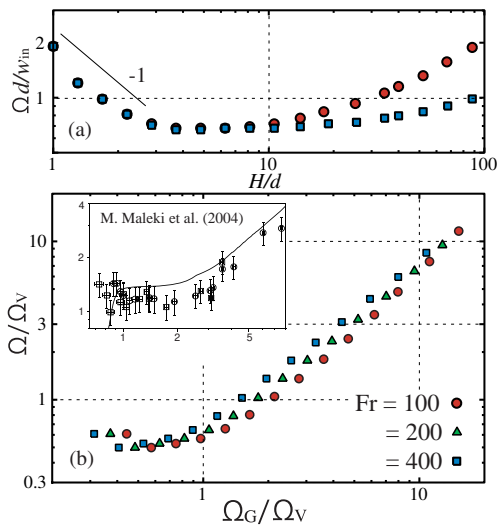


FIG. 3: Transition from viscous to gravitational coiling for  $Fr = 100, 200$  and  $400$ . (a) Dimensionless frequency  $\Omega d/w_{in}$  versus height in condition of  $Re = 3$ . (b) Frequency-height curve rescaled using the  $\Omega_V$  and  $\Omega_G$ . The inset shows the experimental result by M. Maleki *et. al.* [4].

[1, 2, 3, 4, 5] or the rope's radius [6]. Let us compare the coiling frequency of the present model with the experiments. To investigate the viscous coiling regime as a first step,  $Fr$  is set to a very large value, since the viscous coiling takes place when the effect of gravity is small. Figure 3(a) shows a dimensionless frequency  $\Omega d/w_{in}$  as a function of fall height. We found that  $\Omega \propto H^{-1}$  for lower fall heights, which agrees with the scaling relation in viscous coiling. For  $H/d \simeq 10$ , the frequency is almost constant. This behavior corresponds to the gravitational coiling, because the rope's radius hardly depends on the fall height. In figure 3(b), the frequency-height curves are rescaled with  $\Omega_V$  and  $\Omega_G$  in order to compare the results with the experiment by M. Maleki *et. al.* (see the inset). The transition from viscous to gravitational coiling occurs at  $\Omega_G/\Omega_V \simeq 1$ . These results are in good agreement with the experiments including the transient regimes. For a higher fall height of  $H \simeq 10^2$ , the frequency increases as  $\Omega \propto H$ , which agrees with the earliest observation by G. Barnes and J. MacKenze [1, 2].

Supposing strong stretching  $a \ll d$  due to gravity, the scaling relation Eq. (3) predicts  $\Omega \propto H^{10/3}$  [5]. In this case, we reasonably choose a characteristic time scale  $\sqrt{d/g}$ . According to simple dimensional arguments [3], frequency  $\Omega\sqrt{d/g}$  must have the form:

$$\Omega\sqrt{d/g} = f\left(\frac{\nu Q}{gd^4}, \frac{gd^3}{\nu^2}, \frac{H}{d}\right), \quad (12)$$

where  $\nu = \eta/\rho$  is the kinematic viscosity. Here it is noticed that the first parameter in this function is the ratio of the viscous force to the gravitational force  $F_V/F_G$ , the second is the ratio of the gravitational force times the inertia force to the viscous force  $F_G F_I/F_V^2$ , and the third

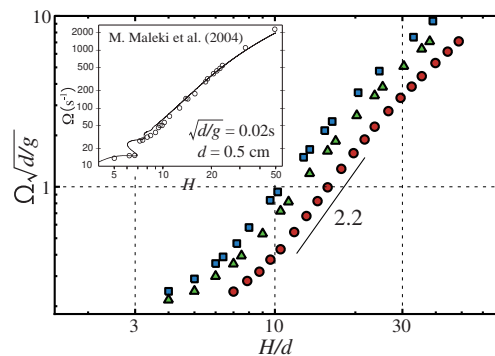


FIG. 4: Dimensionless frequency  $\Omega\sqrt{d/g}$  versus height obtained from the present model. Parameters are:  $\nu Q/gd^4 = 0.2$  and  $gd^3/\nu^2 = 0.2$  (open circle),  $\nu Q/gd^4 = 0.3$  and  $gd^3/\nu^2 = 0.3$  (triangle) and  $\nu Q/gd^4 = 0.2$  and  $gd^3/\nu^2 = 0.5$  (rectangle). The inset shows the experimental result by M. Maleki *et. al.* [4].

is the slenderness ratio. Because the strong stretching condition requires  $F_V/F_G \ll 1$ , the inertial coiling regime appears in the condition:

$$\frac{\nu Q}{gd^4} \sim \frac{gd^3}{\nu^2} \ll 1. \quad (13)$$

Experimentally, Cruickshank and Munson first found  $\Omega \propto H^2$  for  $H/d$  higher than 10, in the condition of  $\nu Q/gd^4 \simeq 0.1-1.7$ ,  $gd^3/\nu^2 \simeq 0.1$  [3]. Ribe also observed  $\Omega \propto H^{2.5}$  for  $gd^3/\nu^2 \simeq 10^{-3}$  and  $\nu Q/gd^4 \simeq 0.5$  [4].

As shown in Fig. 4, the present model gives  $\Omega \propto H^{2.2}$  for the similar conditions. These experimental and theoretical results are successfully consistent. On the other hand, in the gravitational to inertial transitional range, the experiment shows a remarkable discontinuous jump in the frequency (inset in Fig. 4). The present model, though, does not reproduce this behavior.

Next, let us discuss critical fall height  $H^*$ , around which coiling frequency changes from decrease to increase (transition from viscous coiling to gravitational coiling). In figure 3(a), the transition occurs at  $H^* \simeq 6d$ . However, the  $H^*$  should generally be a function of viscosity and gravitational acceleration. For the first step, we focus on the position  $z = \zeta$  at which the flow velocity  $w$  reaches a maximum. Note that, fluid rope changes from tension to compression at this point. After a flow reaches steady state, it is observed that  $\zeta$  hardly depends on time, even though the rope is oscillating. In Fig. 5(a), we plot  $\zeta$  at steady state as a function of fall height. For a shorter fall height, the  $\zeta$  is equal to  $H$ . This indicates that the maximum of  $w$  appears at the point of injection and the fluid rope is wholly compressed. Comparing  $\zeta$  with the frequency  $\Omega d/w_{in}$  shown in Fig.5(b), we can find that the frequency decreases only when the relation  $\zeta = H$  occurs. Therefore, viscous coiling appears in the case in which the whole the rope is compressed. Because this feature can be seen for a wide range of  $Re$  and  $Fr$  as long

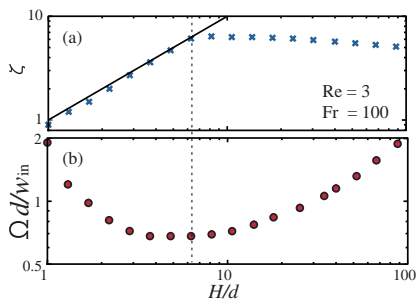


FIG. 5: (a) Numerically calculated value of  $z_c$  for  $Re = 3$  and  $Fr = 100$ . The solid line is the plot of  $\zeta = H$ . (b) Same data with Fig. 3 for comparison.

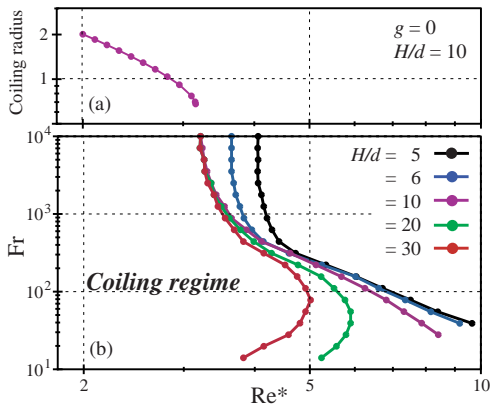


FIG. 6: (a) Numerically calculated coiling radius just below the coil-uncoil transition under no gravity condition. (b) Steady state phase diagram of coiling and uncoiling regime for  $H/d = 5, 10$  and  $15$ .

as the viscous coiling regime exists, we claim that the  $H^*$  is identical to the maximum of  $\zeta$ . The maximum of  $\zeta$  can be realized as a relaxation length of which the effect of boundary condition at  $z = 0$  can travel through a rope. Using  $g$  and  $\nu$ , we can uniquely construct a dimension of length as  $g^{-1/3}\nu^{2/3}$ . Therefore,

$$H^* = \max(\zeta) \propto g^{-1/3}\nu^{2/3}, \quad (14)$$

which is fairly close to the numerically calculated exponents  $\max(\zeta) \propto g^{-0.36}\nu^{0.86}$ .

Finally, we refer to the coil-uncoil transition of the present model. Fluid rope does not coil if Reynolds number is greater than a critical value. Experimentally, in the range of  $Fr \simeq 0.1$  to  $10^4$ , the average value of the critical Reynolds number  $Re^*$  is about 1.2 regardless of the fall height [3]. In the present model, the critical Reynolds number could be a well-defined value because the coiling radius suddenly falls to zero at a certain Reynolds number (Fig. 6(a)). In Figure 6(b), we show a steady state phase diagram of coil-uncoil transition for various fall height. As the  $Fr$  increases, the critical Reynolds number approaches a constant of 3.2, which is independent of fall height for  $H/d > 10$ . We notice that this value  $Re^* = 3.2$  is affected by the parameter appearing in Eq. (11). Decrease of  $Fr$  causes the sharp gradient of flow velocity at the lower part of the rope ( $z < \zeta$ ). This sharp gradient enhances the axial stress  $\sigma_n$ , even though the viscosity is small. The coiling regime therefore expands for lower  $Fr$ . However, for  $H/d = 20$  and  $30$ , the coiling regime shrinks at  $Fr < 10^2$ . This is because the Reynolds number may become very large locally at the bottom of the rope.

In summary, we have proposed a numerical model for fluid rope coiling. The numerical solution of the proposed model reproduces three distinct coiling regimes with the exponent  $\alpha$  of the scaling relation  $\Omega \propto H^\alpha$  as:  $\alpha = -1$  for viscous coiling,  $\alpha = 0$  and  $1$  for gravitational coiling with moderate and higher fall heights, and  $\alpha = 2.2$  for inertial coiling. We phenomenologically argue that the viscous-gravitational transient height  $H^*$  is the height at which the flow velocity reaches its maximum. Based on this hypothesis, we derived a scaling relation for  $H^*$ . The transition from coiling flow to axial stagnation flow occurs with a discontinuous decrease of coiling radius. We obtained a steady state phase diagram for coil-uncoil transition, and found  $Re^* = 3.2$  for  $Fr \gg 1$ .

We would like to thank Dr. Katsuhiko Sato and Dr. Toshihiro Kawakatsu for their critical comments.

- 
- [1] G. Barnes and R. Woodcock, Am. J. Phys. **26**, 205 (1958)
  - [2] G. Barnes and J. MacKenzie, Am. J. Phys. **27**, 112 (1959)
  - [3] J. O. Cruickshank and B. R. Munson, J. Fluid Mech. **113**, 221 (1981)
  - [4] M. Makeki, M. Habibi R. Golestanian, N. M. Ribe and Daniel Bonn, Phys. Rev. Lett. **93**, 214502 (2004)
  - [5] M. Habibi, M. Makeki, R. Golestanian, N. M. Ribe and D. Bonn, Phys. Rev. E **74**, 066306 (2006)
  - [6] L. Mahadevan, W. S. Ryu and A. D. T. Samuel. Nature (London), **392**, 140 (1998); **403**, 502 (2000)
  - [7] J. O. Cruickshank, J. Fluid Mech. **193**, 111 (1988)
  - [8] B. Tchavdarov, A. L. Yarin and S. Radev, J. Fluid Mech. **253**, 593 (1993)
  - [9] N. M. Ribe, M. Habibi and D. Bonn, Phys. Fluids **18**, 084102 (2006)
  - [10] Neil M. Ribe, Proc. R. Soc. Lond. A **460**, 3223 (2004)
  - [11] F. T. Trouton, Proc. R. Soc. Lond. A **77**, 426 (1906)
  - [12] J. O. Cruickshank and B. R. Munson, Phys. Fluids **25**, 1935 (1982)
  - [13] Simulation movies of the present model are available at...